# Interpretation of the pressure-induced Raman frequency shift of the $\nu$ 1 stretching bands of CH 4 and N 2 within CH4-CO2 , N2-CO2 and CH4-N2 binary mixtures

Van-Hoan Le, Alexandre Tarantola, Marie-Camille Caumon

# Interpretation of the pressure-induced Raman frequency shift of the $\nu_1$ stretching bands of $CH_4$ and $N_2$ within $CH_4$-$CO_2$, $N_2$-$CO_2$ and $CH_4$-$N_2$ binary mixtures

Van-Hoan Le,*[a] Alexandre Tarantola [a] and Marie-Camille Caumon [a]

The relationships between the frequency shift of the $\nu_1$ stretching bands of $CH_4$ and $N_2$ with pressure (or density) and composition has been previously provided in the literature as accurate empirical barometers and densimeters for the direct determination of the pressure or density of gas mixtures. However, the latter results still remain a pure description of the experimental data without any interpretation of the physical mechanisms hidden behind the variation trend of the observed peak position. The present paper is devoted to interpreting the origin of the pressure-induced vibrational frequency shifts of the $\nu_1$ stretching bands of $CH_4$ and $N_2$ within $CH_4$-$CO_2$, $N_2$-$CO_2$ and $CH_4$-$N_2$ binary mixtures at the molecular scale. Two different theoretical models (i.e., the Lennard-Jones 6-12 potential approximation - LJ, and the generalized perturbed hard-sphere fluid - PHF) are used to intuitively and qualitatively assess the variation trend as well as the magnitude of the frequency shift of the $CH_4$ and $N_2$ $\nu_1$ bands for an in-depth understanding. Thereby, the contribution of the attractive and repulsive solvation-mean forces to the variation of the Raman frequency shift as a function of pressure and composition is assessed. A predictive model of the variation trend of the frequency shift of the $CH_4$ $\nu_1$ band as a function of pressure (up to 3000 bars), density and composition within $CH_4$-$N_2$ and $CH_4$-$CO_2$ binary mixtures is then provided.

Keywords: Raman spectroscopy, frequency shift, intermolecular interaction, Lennard-Jones potential, Perturbed Hard-Sphere fluid model.

## 1 Introduction

Raman spectroscopy is a straightforward analytical tool to quickly identify the chemical nature of substances based on their vibrational frequency fingerprints.[1,2] The latter can be slightly perturbed by the interaction of the molecule with its medium under the effect of pressure, density, temperature, and/or composition,[3] reflecting a small yet measurable and reproducible shift from their original position measured at low density (pressure). Thus, interpretation and determination of the Raman frequency shifts may provide a direct proxy for investigating physicochemical and thermodynamic properties of fluids, including solute-solvent coupling mechanisms and intermolecular interaction forces.[4,5]

Beside $CO_2$, $CH_4$ and $N_2$ are among the most common volatile species ubiquitous in various geological environments.[6–9] Their pressure-induced Raman frequency shift has been intensively studied since the 1970s to develop barometers and densimeters.[10–13] Most studies investigated pure components without fully considering the significant and systematic effect of composition in the variation of the $CH_4$ and $N_2$ peak position, which was however experimentally revealed in numerous works.[11,14,15] Recently, Le et al.[16,17] presented a new calibration data based on the variation of the band position of $CH_4$ and $N_2$ in pure gas systems, and binary and ternary mixtures of $CH_4$-$CO_2$-$N_2$. The wavelength shifts of the $CH_4$ $\nu_1$ band were then used as a reliable parameter for the development of accurate barometer and densimeter. The measurement of the $N_2$ band peak position was however shown to be less reproducible than that of $CH_4$ due to its asymmetric shape at low pressure and the overlapping with the signal of atmospheric nitrogen.[16,17] Still, the frequency shift of the $N_2$ band was used to provide accurate quantitative calibration data for $CO_2$-$CH_4$-$N_2$ systems by Sublett et al.[18] The above-mentioned works were mainly dedicated to providing accurate experimental calibration data of the Raman signal based on the variation of peak position for direct applications in the quantitative measurement of *PVTX* properties. Thus, the pressure-induced vibrational frequency shift of $CH_4$ and $N_2$ bands was principally described rather than interpreted from a chemical-physical point of view.

Lennard-Jones 6-12 potential approximation (LJ)[19] and the generalized perturbed hard-sphere fluid model (PHF)[5,20] are theoretical models describing the evolution of the repulsive and attractive intermolecular interaction forces that contribute to the resulting Raman frequency shift as a function of pressure, density and/or intermolecular distance. The PHF model was successfully tested for studying the frequency shift of the $\nu_1$ band of pure $N_2$ and $CH_4$ as a function of density and temperature.[21] The results showed a good correlation between the predicted and experimental frequency shifts. It is to note that Ben-Amotz et al.[21] treated the attractive force-induced frequency shift of the $CH_4$ $\nu_1$ band as a linear density-dependent one (according to the mean-field approximation of the van der Walls equation of state[5]). However, more recent experimental results suggested that the attractive force-induced frequency shift of the vibrational modes involving hydrogen bonds (e.g., O–H or C–H bonds) varies nonlinearly as a function of density rather than linearly, especially at high density or pressure.[20,22] Besides, a noticeable difference between the variation trend of the $\nu_1$ band of $CH_4$ in $CH_4$-$N_2$ and $CH_4$-$CO_2$ mixtures was observed [14,15,17] and so needs to be interpreted from a chemical-physical point of view.

The present study aims to interpret the fundamental mechanism hidden behind the observed Raman frequency shift of the $CH_4$ and $N_2$ $\nu_1$ bands and their variation trends as a function of pressure, density and composition. The LJ model is firstly used to intuitively interpret the global variation trend of

the pressure-induced frequency shift ($\Delta\nu$) of the $CH_4$ and $N_2$ bands in pure and binary mixtures of $CH_4$-$CO_2$-$N_2$ without any complex molecular dynamic simulation or *ab-initio* calculations. The variation of $\Delta\nu$ is therefore reasonably explained by attributing them to the variation of the LJ potential. For evaluating the contribution of the repulsive and attractive solvation mean-forces as a function of pressure, density and composition (mol%), the net frequency shift of the $CH_4$ $\nu_1$ band is quantitatively decomposed into the repulsive and attractive components using the PHF model (that of $N_2$ band is not studied herein due to the lack of accurate experimental data within binary mixtures). For that, the non-linearity of the attractive force-induced frequency shift of the $CH_4$ $\nu_1$ band is evaluated. New attractive coefficient parameters ($C_a$, $B_a$) required upon the application of the PHF model are then provided by fitting our experimental data. Afterwards, the predictive model of the variation trends of the $CH_4$ $\nu_1$ band position within $CH_4$-$N_2$ and $CH_4$-$CO_2$ mixtures over 5-3000 bars is provided.

## 2 Experimental data

Experimental data of the pressure-induce frequency shift of $CH_4$ and $N_2$ $\nu_1$ bands within pure or binary mixtures of $CH_4$-$CO_2$-$N_2$ can be found in literature, e.g., for low pressure range (0-600 bars)[14–17] and high pressure range (up to 3000 bars)[11]. The global variation trend of the $CH_4$ and $N_2$ $\nu_1$ bands with the change of pressure, density and composition revealed by all data sets shows a good agreement. Herein, we are interested in the relative variation of the fitted peak position of the $\nu_1$ stretching band of $CH_4$ and $N_2$ ($\Delta\nu$), which is the difference between the fitted peak position recorded at a given pressure and near-zero pressure (~5 bars), so-called hereafter as "frequency shift". Due to the use of a low spectral resolution (~5 $cm^{-1}$), the data points of Seitz et al.[14,15] are very scattered and even indistinguishable. Thus, the peak position at near-zero pressure cannot be accurately determined. The experimental data of Seitz et al. [14,15] are therefore not used in this study. The experimental data of Sublett et al.[18] were also not considered in this study because they are only reported for ternary mixtures. It is to note that the variation trends of the $CH_4$ and $N_2$ bands within binary and ternary mixtures are different, and the frequency shift of $CH_4$ and $N_2$ within ternary mixtures varies non-systematically with composition variation.[17,18] In this study, the selected data are thus from the works of Le et al. [16,17] (for the pressure between 5-600 bars) and from Fabre and Oksengorn [11] (for pressure up to 3000 bars in $CH_4$-$N_2$ mixtures).

The experimental protocol of the measurements over 5-600 bars is described in Le et al.[16,17] Briefly, binary gas mixtures of any composition are prepared from pure $CH_4$, $CO_2$ and $N_2$ gases (99.99% Air Liquid™) by a commercial mixer (GasMix Alytech™), then compressed by a home-made pressurization system and stored in a stainless steel tanker at ~130 bars. The composition of the obtained gas mixtures, before being loaded in an improved High-Pressure Optical Cell system (HPOC) [23,24], is checked by gas chromatography with an uncertainty of about ± 0.3 mol%. The HPOC system serves as a chamber sample, whose one end is equipped with a manual screw pump for pressure adjustment, and the other end is connected to a sealed transparent microcapillary placed on a Linkam CAP500 heating-cooling stage for temperature control. The temperature is maintained at 22.0 ± 0.1 °C. The internal pressure is monitored by two pressure-transducers (±1 bar). Pressure-to-density conversion is done by REFPROP software[25] using default options of equation of states (EoS), i.e., Setzmann and Wagner[26] and Span et al.[27] for pure $CH_4$ and $N_2$, and GERG-2008 [28] for gas mixtures. Raman spectra are collected with a LabRAM HR spectrometer (Horiba Jobin-Yvon) equipped with a liquid-nitrogen cooling CCD detector, a 514.532 nm $Ar^+$ laser (Stabilite 2017, Spectra-Physics), a ×20 Olympus objective (NA = 0.4) and a 1800 groove·$mm^{-1}$ grating. The confocal hole and the slit are set at 1000 and 200 µm, respectively, yielding a spectral resolution of about 1.6 $cm^{-1}$. The laser power at the sample is ~ 30 mW. At any given *PTX* condition, each Raman measurement (with 10 accumulations) is repeated at least six times for statistical purpose. Accumulation time is between 2 and 15s depending on pressure. The uncertainty of the measured frequency shift is about 0.02 $cm^{-1}$. The Raman spectra are fitted with Labspec6 software (Horiba), after baseline correction, using asymmetric Gaussian-Lorentzian function (for $N_2$ band) and symmetric Gaussian-Lorentzian function (for $CH_4$ band). To minimize the day-to-day spontaneous deviation arising from the instrumental response [17,18,29], the whole analysis series of a specific mixture must be continuously performed and done within the same experimental section.

On the other hand, the calibration data of Fabre and Oksengorn [11] were performed at room temperature only for pure $CH_4$, $N_2$ and a commercial gas mixture of $CH_4$-$N_2$ (55/45 ± 3 mol%, respectively) for pressures up to ~ 3000 bars. Raman spectra were collected using a 488 nm Ar-ion laser. The spectral resolution was about 0.8 $cm^{-1}$. The experimental protocol and other spectral parameters (objective, grating, confocal hole and slit size, etc.) were not detailed.

## 3 Background theory

### 3.1 The Lennard-Jones (LJ) potential approximation.

The Lennard-Jones 6-12 potential ($U_{LJ}$) approximation describes the evolution of the repulsive and attractive potentials experienced between two molecules as a function of their intermolecular distance *r*.[19] The general mathematic form of $U_{LJ}$ is expressed by Eq. 1, where the parameters $\sigma$ and *r* have the dimension of a length (Å), and the attraction parameter $\varepsilon$ and $U_{LJ}$ are expressed in joule (J).

$$\mathbf{U_{LJ}} = \mathbf{4}\varepsilon\left(\left(\frac{\sigma}{\mathbf{r}}\right)^{\mathbf{12}} - \left(\frac{\sigma}{\mathbf{r}}\right)^{\mathbf{6}}\right) \quad (1)$$

Figure 1 represents the relative variation of $U_{LJ}$ as a function of the distance between two identical molecules of $CH_4$. For a pair of non-identical molecules, $U_{LJ}$ can be estimated from parameters $\sigma_{ij}$ and $\varepsilon_{ij}$ determined using Lorentz-Berthelot combining rules (Eq. 2 and 3). LJ parameters of $CH_4$, $N_2$ and $CO_2$ are all listed in Table 1. [30,31]

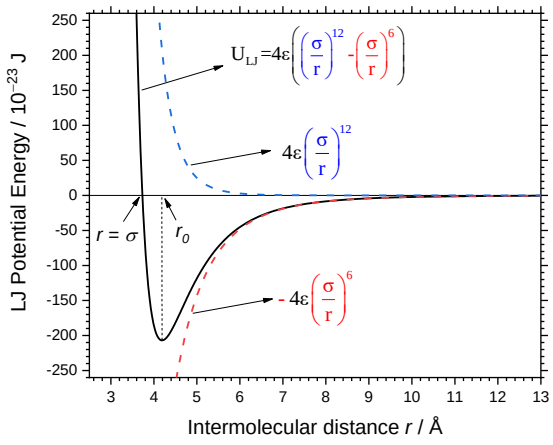


Figure 1: Lennard-Jones 6-12 potential between two $CH_4$ molecules as a function of intermolecular distance *r*.

$$\sigma_{ij} = \frac{\sigma_i + \sigma_j}{2} \quad (2)$$

$$\varepsilon_{ij} = \sqrt{\varepsilon_i \varepsilon_j} \quad (3)$$

Table 1: LJ parameters between two identical or non-identical molecules of $CH_4$, $N_2$ and $CO_2$. $k_B$ is Boltzmann constant (J/K)

| Molecular pair | σ (Å) | $\varepsilon/k_B$ (K) |
|---|---|---|
| $CH_4$-$CH_4$ | 3.733 | 149.9 |
| $N_2$-$N_2$ | 3.745 | 95.2 |
| $CO_2$-$CO_2$ | 3.713 | 257.8 |
| $CH_4$-$N_2$ | 3.739 | 119.5 |
| $CH_4$-$CO_2$ | 3.723 | 196.6 |

The net $U_{LJ}$ can be decomposed into repulsive and attractive components (cf. Eq. 1 and Figure 1). In general, at very low pressure (low density) where the intermolecular distance *r* is large enough (> 9Å), there is no interaction between molecules. As pressure increases, the distance between molecules is reduced, and so molecules begin to interact with each other with more frequent collisions and steric restrictions. At long distance-range, the attractive force dominates and produces a significant effect, whereas the repulsive forces are negligible. The net $U_{LJ}$ reaches its minimum value at the intermolecular distance $r_0 = 1.1224\sigma$. At $r = \sigma$, the repulsive force completely compensates the attractive force, i.e., the net $U_{LJ}$ equals zero. For small intermolecular distances, the repulsive force dominates the interactions (Figure 1).

Since $CH_4$, $N_2$ and $CO_2$ are all non-polar molecules, the effects of the electrostatic and the polarization potential energy on the actual potential energies within the binary systems may be negligible (Coulomb's law). In other words, the intermolecular interactions experienced between these molecular pairs chiefly consist of repulsive and attractive forces. The LJ potential approximation could therefore be used to reasonably interpret the overall fashion of the variation trend of the pressure-induced frequency shifts of the mentioned gaseous systems. The variation of the intermolecular interaction impacts the vibrational mode of gaseous molecules by different phenomena such as lengthening or shortening of bond length or perturbing electron cloud distribution, and so resulting in polarizability changes. In general, the attractive forces expand the geometry and so the bond length of molecules, implying that less energy is required to stretch the bonds[4,32,33] which result in a redshift. On the contrary, the repulsive force producing more significant effect at short distance range tend to contract the geometry of molecules, and so the bond length. The observed vibration mode requires therefore more energy, which in turn leads to a blueshift.[4,32,33]

### 3.2 Perturbed hard-sphere fluid model

Based on the theoretical model developed by Buckingham[4], the relationship between vibrational frequency shifts ($\Delta\nu$) and medium-induced intermolecular forces experienced along the bond is represented by Eq. 4, [32,34] where $\nu_0$ is the unperturbed vibrational frequency measured at low density; *f* and *g* are the harmonic and anharmonic force constants of an isolated diatomic solute (Eq. 5); F and G are the linear and quadratic coefficients in an expansion of the solvent potential of mean-force as a function of solute bond length (Eq. 6); and $f_1(\kappa)$ and $f_2(\kappa)$ are the modified Morse coefficients for anharmonic vibration. [35,36,34]

$$\Delta\nu \approx \nu_0 \frac{F}{f}\left[-\left(\frac{3g}{2f}\right) f_1(\kappa) + \left(\frac{G}{F}\right) f_2(\kappa)\right] \quad (4)$$

$$U_0(r_{12}) = \frac{1}{2} f (r_{12} - r_e)^2 + \frac{1}{2} g (r_{12} - r_e)^3 + \cdots \quad (5)$$

$$V_{mean-force} = F(r_{12} - r_e) + G(r_{12} - r_e)^2 + \cdots \quad (6)$$

The net frequency shift $\Delta\nu$ can be decomposed into the repulsive ($\Delta\nu_R$) and attractive ($\Delta\nu_A$) contributions, which are induced by repulsive and attractive solvation-mean forces, respectively (Eq. 7). The centrifugal forces only show a noticeable effect at ultrahigh pressure (e.g., ~158 kbar in study of Devendorf et al. [37]). It is therefore negligeable in this study.

$$\Delta\nu = \Delta\nu_R + \Delta\nu_A \quad (7)$$

The repulsive contribution ($\Delta\nu_R$) can be accurately calculated from PHF model parameters.[5,20,21,32] All required hard-sphere parameters of solute $CH_4$ and solvent ($CH_4$, $N_2$ and $CO_2$) are reported in Table 2. The detailed calculation process can be found in Ben-Amotz et al. 1993.[20]

On the other hand, the attractive contribution ($\Delta\nu_A$) within diatomic or pseudoatomic molecules is assumed to be proportional to the attractive force ($F_A$) acting along the vibrational bond.[5] Since $F_A$ varies relatively slowly, Chandler and co-workers assumed that the attractive contribution ($\Delta\nu_A$) varies linearly with the solvent density, i.e., $\Delta\nu_A = C_a \cdot \rho$ (where $C_a$ is an empirical coefficient fitted from experimental data). This assumption had shown a good agreement in various solvent-solute systems.[5,32,21] Recently published experimental data however showed that $\Delta\nu_A$ may rather vary as a quadratic function of density (i.e., $\Delta\nu_A = B_a \cdot \rho^2 + C_a \cdot \rho$) [36,20,38–41], especially for hydrogen stretching vibrations (e.g., C–H, O–H). The parameters $C_a$ and $B_a$ can also be empirically fitted from experimental data. Once these adjustment parameters are determined, the attractive frequency shift $\Delta\nu_A$ can be calculated for any arbitrary density.

Table 2: Hard-sphere fluid parameters of solute ($CH_4$) and solvent ($CH_4$, $N_2$, and $CO_2$) [21].

| bond | $\nu_0$ ($cm^{-1}$) | $r_e$ (Å) | $\sigma_1$ (Å) | $\sigma_2$ (Å) | $\sigma_s^{CH_4}$ (Å) | $\sigma_s^{N_2}$ (Å) | $\sigma_s^{CO_2}$ (Å) | $f$ (dyne/Å) | $g$ (dyne/Å²) |
|---|---|---|---|---|---|---|---|---|---|
| C-H | 2917 | 1.091 | 2.22 | 3.53 | 3.58 | 3.45 | 4.00 | 0.005049 | -0.01047 |

$\nu_0$ : Raman peak position of $CH_4$ $\nu_1$ band at near-zero pressure.

$r_e$ : bond length of $CH_4$ $\nu_1$ band at equilibria.

$\sigma_1$ and $\sigma_2$ : pseudo-diatomic hard-sphere diameters of $CH_4$ solute.

$\sigma_s$ : hard-sphere diameters of solvent.

*f, g* : harmonic and anharmonic force constants of isolated $CH_4$ solute molecule, respectively.

It should be kept in mind that the frequency shift of the $CH_4$ $\nu_1$ band changes not only with different solvents but also gradually changes as a function of the molar fraction (composition).[14–18] Thus, $C_a$ and $B_a$ are also expected to be composition dependent. In this study, both assumptions (linear and quadratic density-dependence of $\Delta\nu_A$) will be examined for the case of $CH_4$ ($\nu_1$ stretching band) dissolved in different solvents (pure $CH_4$, $CH_4$-$N_2$ and $CH_4$-$CO_2$ mixtures). The adjustable parameters $C_a$ and $B_a$ are then provided by fitting selected experimental data.

## 4 Results and discussion

### 4.1 Pressure-induced frequency shift of $N_2$ and $CH_4$ bands

The variation of the peak position of the $\nu_1$ stretching bands of $N_2$ (within the $CH_4$-$N_2$ and $CO_2$-$N_2$ mixtures) and $CH_4$ (within the $CH_4$-$N_2$ and $CH_4$-$CO_2$ mixtures) as a function of pressure and composition was previously reported in the literature[11,14–17] and selectively plotted in Figure 2 and Figure 3.

Briefly, both $N_2$ and $CH_4$ bands shift toward lower wavenumbers as pressure (density) increases. The composition effect is very small at low pressure and becomes more pronounced at high pressure. As evidence, the curves converge to a point at near-zero pressure (low density) and span out as pressure increases (Figure 2 and Figure 3a), except over the pressure range 300 - 400 bars in the case of $CH_4$-$CO_2$ mixtures (Figure 3b). The magnitude of the frequency shift of $N_2$ in $CH_4$-$N_2$ and $CO_2$-$N_2$ mixtures gradually increases with decreasing $N_2$ concentration (Figure 2), whereas that of $CH_4$ band in the $CH_4$-$N_2$ mixtures decreases with decreasing $CH_4$ concentration (Figure 3a). The difference between the propensity of the frequency shift of $CH_4$ in $CH_4$-$N_2$ mixtures and that in $CH_4$-$CO_2$ mixtures can be observed in Figure 3. Indeed, the magnitude of the frequency shift of $CH_4$ within $CH_4$-$CO_2$ mixtures may increase or decrease as $CH_4$ concentration decreases, depending on the pressure-range.

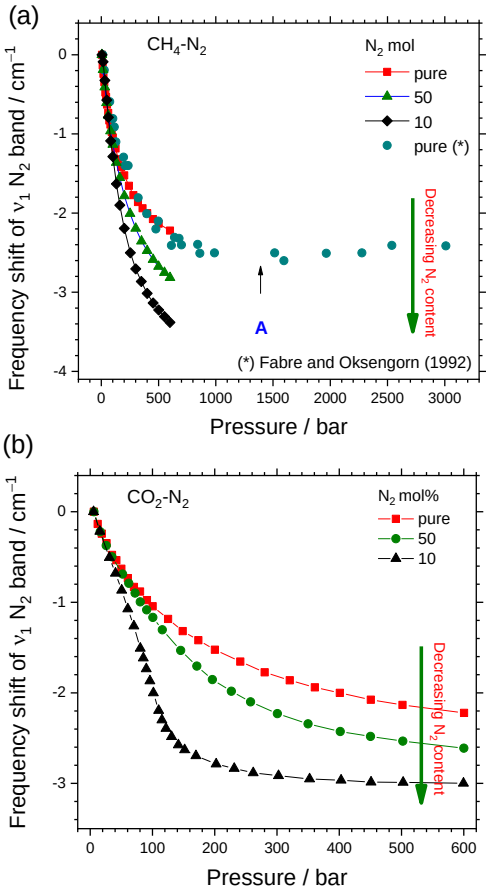


Figure 2: Frequency shift of the ν1 stretching band of N2 measured at 22 °C as a function of pressure and composition in (a) $CH_4$-$N_2$ and (b) $CO_2$-$N_2$ mixtures. Experimental data are from Le et al. [17] (up to 600 bars) and Fabre et Oksengorn [11] (up to 3000 bars). The frequency shift of the $\nu_1$ band of pure $N_2$ reaches the minimal value within the pressure range ~ 1200 - 1600 bars. Inflection point A is located using LJ potential approximation (see text in section 4.2).

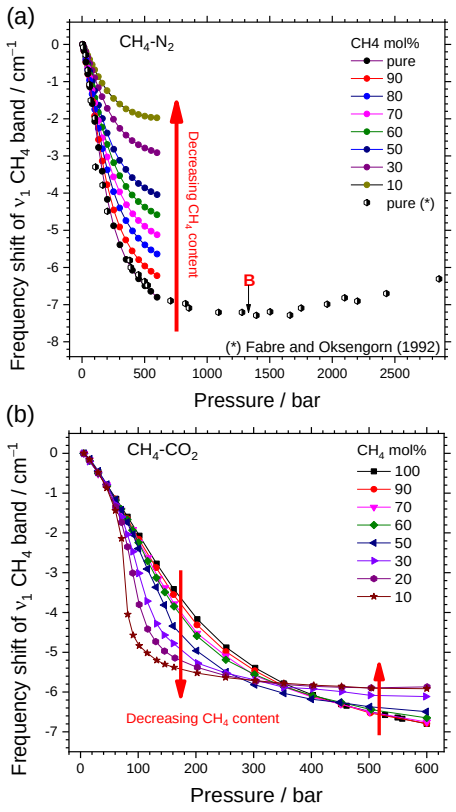


Figure 3: Frequency shift of the $\nu_1$ stretching band of $CH_4$ measured at 22 °C as a function and pressure and composition in (a) $CH_4$-$N_2$ and (b) $CH_4$-$CO_2$ mixtures. Experimental data are from Le et al. [17] (up to 600 bars) and Fabre et Oksengorn [11] (up to 3000 bars). The frequency shift of the $\nu_1$ band of pure $CH_4$ reaches the minimal value within the pressure range ~ 1200 - 1700 bars. Inflection point B is located using LJ potential approximation (see text in section 4.2).

### 4.2 Interpretation of the frequency shift based on the Lennard-Jones potential approximation: effect of pressure (density)

Figure 4a presents the variation of intermolecular distance *r* as a function of pressure of pure $CH_4$ and different mixtures with $N_2$ or $CO_2$ over 5-600 bars. Overall, the curves plotted in Figure 4a show a close affinity with the relative order and the curvature change as a function of composition of the frequency shift-pressure curves plotted in Figure 2 and Figure 3. The intermolecular distance at any pressure decreases from pure $N_2$ to pure $CH_4$ then pure $CO_2$, which is in good agreement with the overall variation trends of the magnitude of the frequency shift of the $N_2$ and $CH_4$ bands as composition varies, i.e., the magnitude of the frequency shift of the $N_2$ band always decreases when it is mixed with either $CH_4$ or $CO_2$ (Figure 2), whereas that of the $CH_4$ band decreases when it is mixed with $N_2$ or increases when it is mixed with $CO_2$ (over ~ 1-400 bars) (Figure 3). The above observation are in good agreement with the interpretation of Sublett et al.[18] where the variation of molar density as a function of pressure and composition is discussed. The curvature of the frequency shift calibration curves of $CH_4$ and $N_2$ bands within $CH_4$-$N_2$ mixtures progressively changes with the change of $CH_4$ or $N_2$ content (Figure 2 and Figure 3a). Regarding $CO_2$-$N_2$ and $CH_4$-$CO_2$ mixtures dominated by $CO_2$ (for example $CH_4$-$CO_2$ mixture of 90 mol% $CO_2$), the intermolecular distance drastically decreases at around 80-150 bars then slowly decreases with further pressure increase. These variation trends reasonably mirror the significant decrease, then followed by a stepwise-like behavior of the curve of the $CH_4$-$CO_2$ mixture of 90 mol% $CO_2$ as observed in Figure 3b. Similar variation is observed for the curve of the $CO_2$-$N_2$ mixture of 90 mol% $CO_2$ Figure 2b). The similarity described above is thus an evidence of the intrinsic correlation between the observed Raman frequency shifts and the intermolecular distance change, as well as the variation of intermolecular interactions. Thus, the LJ potential may be used to practically interpret the observed pressure-induced Raman frequency shift.

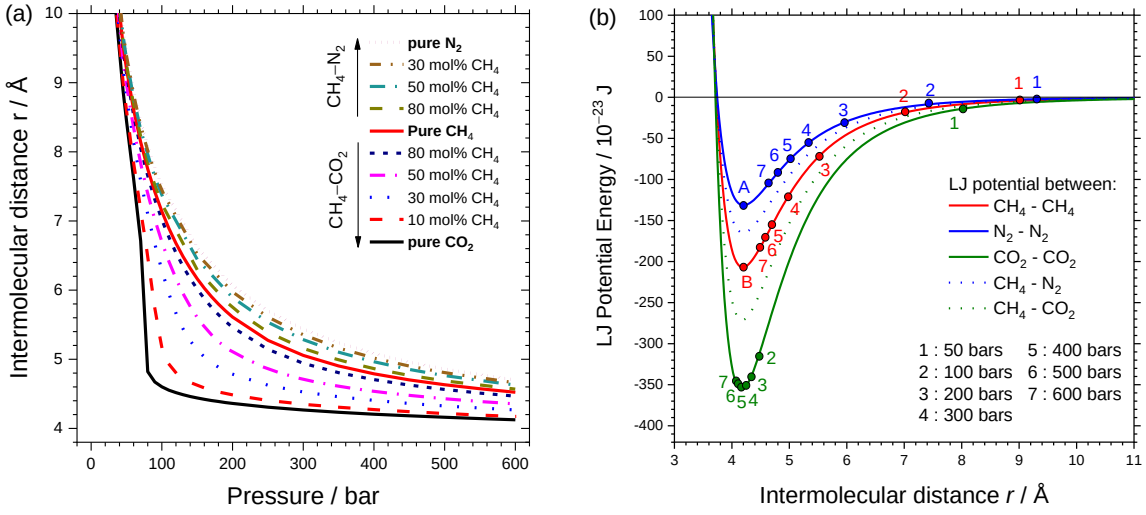


Figure 4: (a) Variation of the intermolecular distance *r* (Å) as a function of pressure of pure $CH_4$ and in mixtures with $CO_2$ or $N_2$. The intermolecular distance *r* between $CH_4$ and/or $N_2$ molecules was calculated by the cube root of the density. Pressure-to-density conversion is done by REFPROP software. (b) Variation of Lennard-Jones 6-12 potential experienced between a pair of identical molecules of $CH_4$, $N_2$ and $CO_2$ (solid lines) or a pair of non-identical molecules, i.e., $CH_4$-$N_2$ or $CH_4$-$CO_2$ (dotted-lines). The points A (~ 1400 bars) and B (~ 1300 bars) are the minimal value when $r_0 = 1.1224\sigma$.

Figure 4b shows how $U_{LJ}$ between a pair of two (identical or non-identical) molecules of $CH_4$, $N_2$, and $CO_2$ varies as a function of intermolecular distance *r* and pressure (represented by solid points denoted 1 to 7). The $U_{LJ}$ becomes more and more negative with increasing pressure, implying a domination by attraction forces, so resulting in a continuous downshift of $CH_4$ and $N_2$ bands. With a further increase of pressure, the intermolecular distance reaches the value $r = r_0$ where the $U_{LJ}$ of $N_2$ and $CH_4$ are minimal, marked by points A and B at ~ 1400 and 1300 bars, respectively (density-to-pressure conversion is done by REFPROP program). At these points, the effect of the repulsive potential to frequency shift balances that induced by attractive potential. Correspondingly, an inflection is observed on the experimental frequency shift-pressure curves at around ~ 1200-1600 bars for pure $N_2$ and ~ 1200-1700 bars for pure $CH_4$ (Figure 2 and Figure 3a), e.g., pressure ranges where points A and B marked in Figure 4b are found. Afterward, the $CH_4$ and $N_2$ bands undergo a blueshift as the onset of the important contribution of repulsive potential.

The downshift magnitude of the $CH_4$ band is more significant than that of $N_2$ at any pressure and composition (e.g., ~ −6.8 and −2.1 $cm^{-1}$ at 600 bars, respectively, cf. Figure 2 and Figure 3). It can be directly explained by the fact that the derivative of the polarizability of vibrational coordinate ($d\alpha/dQ$) for the C−H bond within $CH_4$ molecules is much larger than that of the N−N bond within $N_2$ molecules (e.g., 2.08 in $CH_4$ > 0.66 in $N_2$,[42]). The magnitude of $U_{LJ}$ potentials shown in Figure 4b also reasonably reflects the relative difference between the downshift magnitude of $CH_4$ and $N_2$ bands within pure systems or $CH_4$-$N_2$ mixtures.

However, the LJ 6-12 potential approximation could not interpret quantitatively the downshift magnitude of the $CH_4$ band in $CH_4$-$CO_2$ mixtures. For instance, over 350-600 bars (cf. points 5, 6, and 7 in Figure 4b), the $U_{LJ}$ between $CH_4$ molecules in pure $CH_4$ is much smaller than that between molecules in $CH_4$-$CO_2$ mixtures, but the frequency shift magnitude of the $CH_4$ band within pure $CH_4$ is always larger than that within $CH_4$-$CO_2$ mixtures (Figure 3b). It is noteworthy that the LJ potential approximation only describes the variation between two molecules, whereas the Raman frequency shift of the observed vibration mode chiefly arises from the perturbation caused by its medium (i.e., all surrounding molecules). Therefore, the effective effect of the composition change could not fully be taken into account by the LJ potential approximation. Moreover, the effect of the perturbation also strongly depends on the geometrical configuration between molecules [43], and so on the mixture composition (Figure 2 and Figure 3). Thus, to quantitatively appraise the pressure-induced frequency shift with composition, the solvation mean-forces acting along the vibration bond of the analyzed molecules must be considered using a more appropriate model such as the perturbed hard-sphere fluid model (PHF). Since the calibration data of the $N_2$ $\nu_1$ band within binary mixtures is less reproducible (with no systematic variation with composition)[16,17], in the following, the PHF model is only used to accurately determine the contribution of repulsive and attractive mean-forces to the observed frequency shift of the $CH_4$ band as a function of pressure (density) and composition.

### 4.3 Decomposition of the observed pressure-induced frequency shift into attractive and repulsive components

Figure 5 represents the repulsive and attractive force-induced frequency shifts ($\Delta\nu_R$ and $\Delta\nu_A$, respectively) and the net frequency shift ($\Delta\nu = \Delta\nu_R + \Delta\nu_A$) of the $CH_4$ $\nu_1$ band as a function of density within a pure $CH_4$ gas system. $\Delta\nu_R$ (blue solid line) was determined using the PHF model, whereas $\Delta\nu_A$ was fitted from experimental data by the two following assumptions: (i) linear (green solid line, $\Delta\nu_A^1$) or (ii) quadratic (red solid line, $\Delta\nu_A^2$) equation function of density. The intercept of the regression equations was set to 0 at the lowest density value. Thereby, the net predicted frequency shift $\Delta\nu^1$ and $\Delta\nu^2$ are correspondingly the products of $\Delta\nu_R$ with $\Delta\nu_A^1$ or $\Delta\nu_A^2$, presented in Figure 5 by black solid-curve or dashed solid-curve, respectively. The experimental data of the net frequency shift ($\Delta\nu^{exp}$) over 5 - 3000 bars are also presented in Figure 5.

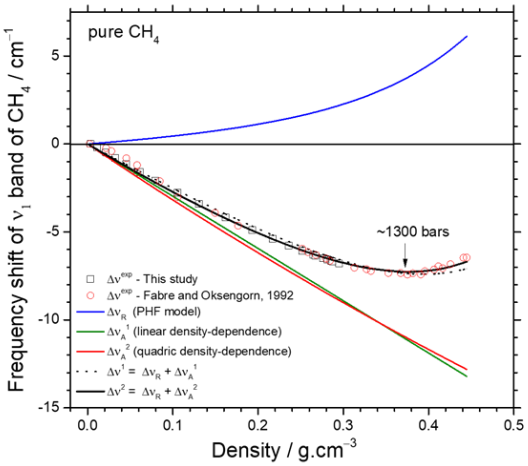


Figure 5: Variation of the frequency shift of the $\nu_1$ band of $CH_4$ measured at 22 °C as a function of density. Experimental data ($\Delta\nu^{exp}$) performed at 5-3000 bars are from literature [11,17]. The repulsive force-induced frequency shift ($\Delta\nu_R$) was calculated using the PHF model. The attractive force-induced frequency shift ($\Delta\nu_A^1$ and $\Delta\nu_A^2$) were fitted from experimental data by a linear or quadratic function, respectively. The net predicted frequency shift ($\Delta\nu^1$ and $\Delta\nu^2$) is the sum of the $\Delta\nu_R$ and $\Delta\nu_A^1$ or $\Delta\nu_A^2$.

Comparing between the linear and quadratic regressions, the resulting $\Delta\nu^1$ and $\Delta\nu^2$ are in good agreement at low-density range (< ~ 0.4 g·$cm^{-3}$), then it starts to slightly deviate at higher density range (Figure 5). The $\Delta\nu^{exp}$ confirmed that the quadratic function describes slightly more accurately the density dependence of $\Delta\nu_A$ than the linear one. It is to note that the small discrepancy between the fitted curves of the linear and quadratic attractive frequency shift models can be improved by adjusting the approximated effective diameters of the solute molecule ($\sigma_1$ and $\sigma_2$) by about 10-20%. In this study, the quadratic function is then used to fit our experimental data of $CH_4$-$N_2$ and $CH_4$-$CO_2$ binary mixtures. All resulting parameters $C_a$ and $B_a$ are listed in Table 3. The adjusted-$R^2$ of the least-square regression is always higher than 0.997.

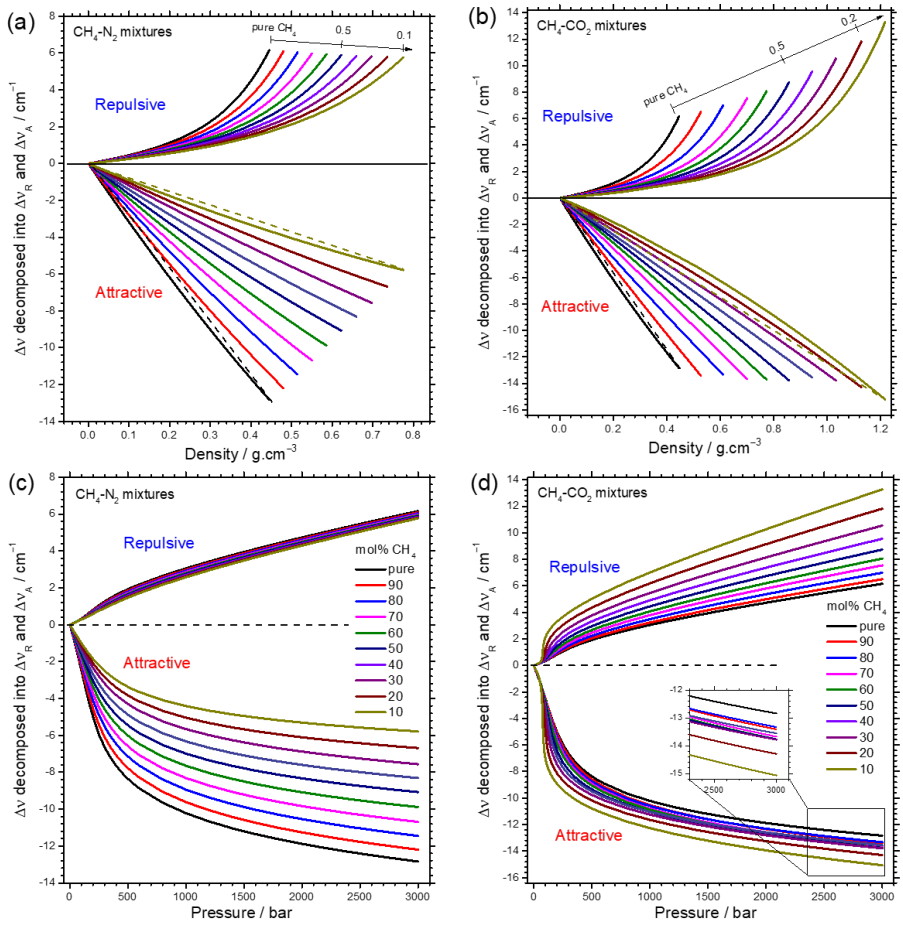


Figure 6: Variation of repulsive and attractive components ($\Delta\nu_R$ and $\Delta\nu_A$) decomposed from the net frequency shift of the $\nu_1$ band of $CH_4$ as a function of composition of $CH_4$-$N_2$ and $CH_4$-$CO_2$ binary mixtures and density (a, b) or pressure (c, d). Dashed straight lines in Figures a and b are guides for eye for curvature evaluation.

Table 3: $\Delta\nu_A$ attractive force parameters of the $CH_4$ band within $CH_4$-$N_2$ and $CH_4$-$CO_2$ binary mixtures, with $\Delta\nu_A = B_a \cdot \rho^2 + C_a \cdot \rho$.

| mol% $CH_4$ | $CH_4$-$N_2$ mixtures | | $CH_4$-$CO_2$ mixtures | |
|---|---|---|---|---|
| | $B_a$ | $C_a$ | $B_a$ | $C_a$ |
| 100 | 8.633 | -32.660 | 8.633 | -32.660 |
| 90 | 6.824 | -28.686 | 1.945 | -26.473 |
| 80 | 5.257 | -24.946 | 1.928 | -23.019 |
| 70 | 4.856 | -22.106 | -0.904 | -18.888 |
| 60 | 4.335 | -19.413 | -1.420 | -16.637 |
| 50 | 3.873 | -16.987 | -1.136 | -15.100 |
| 40 | 2.828 | -14.468 | -0.662 | -13.739 |
| 30 | 1.793 | -12.904 | -1.361 | -11.944 |
| 20 | 2.121 | -10.645 | -2.147 | -10.254 |
| 10 | 2.337 | -9.275 | -3.370 | -8.405 |

The variation of $\Delta\nu_R$ and $\Delta\nu_A$ components decomposed from the net $\Delta\nu$ of the $CH_4$ $\nu_1$ band as a function of density and composition of $CH_4$-$N_2$ and $CH_4$-$CO_2$ mixtures are presented in Figure 6a and b. Both $\Delta\nu_R$ and $\Delta\nu_A$ change gradually with the variation of density and composition as expected. The value of $\Delta\nu_A$ is always greater than $\Delta\nu_R$ at any given density-composition condition, which is in good agreement with the resulting redshift observed in Figure 3. Over the studied density range, the highest value of $\Delta\nu_R$ within $CH_4$-$N_2$ mixtures only shows a subtle change from +6.2 to +5.8 $cm^{-1}$, whereas that in $CH_4$-$CO_2$ mixtures steadily increases from +6.2 to +13.3 $cm^{-1}$ as the content of $CH_4$ decreases. An inverse variation trend is observed for the absolute value of the attractive component $|\Delta\nu_A|$, with a progressive decrease in the $CH_4$-$N_2$ mixtures (from about $-12.9$ to $-5.8$ $cm^{-1}$) but a slight increase in the $CH_4$-$CO_2$ mixtures (from about $-12.9$ to $-15.1$ $cm^{-1}$) as the $CH_4$ content decreases.

The curvature of $\Delta\nu_A$-density curves systematically changes from positive (for $CH_4$-$N_2$ mixtures dominated by $N_2$) to negative (for $CH_4$-$CO_2$ mixtures dominated by $CO_2$) fashion (cf. Figure 6a and b, and coefficient $B_a$ in Table 3). The degree of the nonlinear density dependence of $\Delta\nu_A$ likely depends on the critical temperatures ($T_c$) of the analyzed mixtures. Indeed $T_c$ of pure $N_2$, $CH_4$ and $CO_2$ are $-146.5$, $-82.6$ and 31.05 °C, respectively (cited form NIST Chemistry webbook[44]). Consequently, the $T_c$ of $CH_4$-$N_2$ mixtures, which varies between $-146.5$ and $-82.6$ °C depending on mixture composition, is far lower than room temperature. Thereby, $CH_4$-$N_2$ mixtures are always in supercritical state upon the Raman analyses performed at 22 °C.

On the other hand, the $T_c$ of $CH_4$-$CO_2$ mixtures, which ranges from −82.6 to 31.05 °C as a function of composition, can be closer to the temperature of analysis at 22 °C.

The deviation of the density-dependence of $\Delta\nu_A$ from the linear variation trend could also be ascribed to the aggregation of "non-identical" molecules. Indeed, the uniform molecular distribution may cause less attractive force than the non-uniform one.[40] When compared with the diameter of a $CH_4$ molecule (3.8 Å), the diameter of a $N_2$ molecule (3.65 Å) is rather similar, whereas that of $CO_2$ molecule is significantly smaller (3.3 Å). As a result, the nonlinearity of the density-dependence of $\Delta\nu_A$ in $CH_4$-$N_2$ mixtures is less noticeable than that observed for $CH_4$-$CO_2$ mixtures (Figure 6a and b).

The origin of the difference on the variation trend of the frequency shift of $CH_4$ $\nu_1$ band reported in Figure 3a and b can be better understood by evaluating the variation of $\Delta\nu_R$ and $\Delta\nu_A$ components represented in pressure scale (Figure 6c and d). Regarding $CH_4$-$N_2$ mixtures, $\Delta\nu_R$ is likely unchanged, whereas $\Delta\nu_A$ significantly and progressively changes with composition. This indicates that the attractive solvation mean-forces is the predominant contribution to the variation trend of the $CH_4$ band position as a function of pressure and composition within $CH_4$-$N_2$ mixtures (Figure 6c). On the contrary, the change of $\Delta\nu_A$ as a function of pressure and composition is quite small in the case of $CH_4$-$CO_2$ mixtures compared to that of the repulsive one (Figure 6d). Thus, the variation of the $CH_4$ band position is chiefly governed by the change of $\Delta\nu_R$ as well as of the repulsive solvation mean-force. Inversely to the variation trend of $\Delta\nu_R$ observed in $CH_4$-$N_2$ mixtures, $\Delta\nu_R$ in $CH_4$-$CO_2$ mixtures increases drastically as $CH_4$ content decreases, indicating that the contribution of the solvation mean-force at near-critical temperature becomes somewhat significant.

**4.4 Predictive model of the variation trends of the $\nu_1$ $CH_4$ band**

The net predicted frequency shift $\Delta\nu = \Delta\nu_R + \Delta\nu_A$ (where $\Delta\nu_R$ and $\Delta\nu_A$ are reported in Figure 6) is plotted in Figure 7 as a function of composition and density or pressure, along with experimental data.[11,17] Regarding the $CH_4$-$N_2$ mixtures, the predicted frequency shift curves show a good agreement with experimental data. A slight dispersion is observed for the experimental data of $CH_4$-$N_2$ mixture of 55 mol% $CH_4$ from Fabre et Oksengorn [11]. Indeed, the latter seems to be superimposed to the experimental data of the $CH_4$-$N_2$ mixture of 60 mol% $CH_4$ (Figure 7a). This could partially be explained by the uncertainty of the mixture composition (55 ± 3 and 60 ± 0.5 mol% $CH_4$) and the error of the measured frequency shift (± 0.3 and ± 0.02 $cm^{-1}$ reported in the two studies [11,17], respectively).

Regarding the $CH_4$-$CO_2$ mixtures, the predicted model also shows a good agreement with most experimental data (Figure 7c and d). However, a deviation becomes more appreciable for the mixtures dominated by $CO_2$. The experimental data of the mixtures containing ≤ 40 mol% $CH_4$ start to deviate from the associated predicted curve at high-density range, i.e., near the inflection point of the predicted curves (Figure 7c). A significant discrepancy between experimental data points and the predicted curve is observed for $CH_4$-$CO_2$ mixtures of 10 mol% $CH_4$ at low (~ 0.1 - 0.4 $g{\cdot}cm^{-3}$) and high (> ~ 0.9 $g{\cdot}cm^{-3}$) density ranges, which can be partially ascribed to the inaccuracy of EoS at near critical point, and to the error arising from the quadratic regression due to the blank region (lacking data points) corresponding to the vapor-liquid transition of $CH_4$-$CO_2$ mixtures.

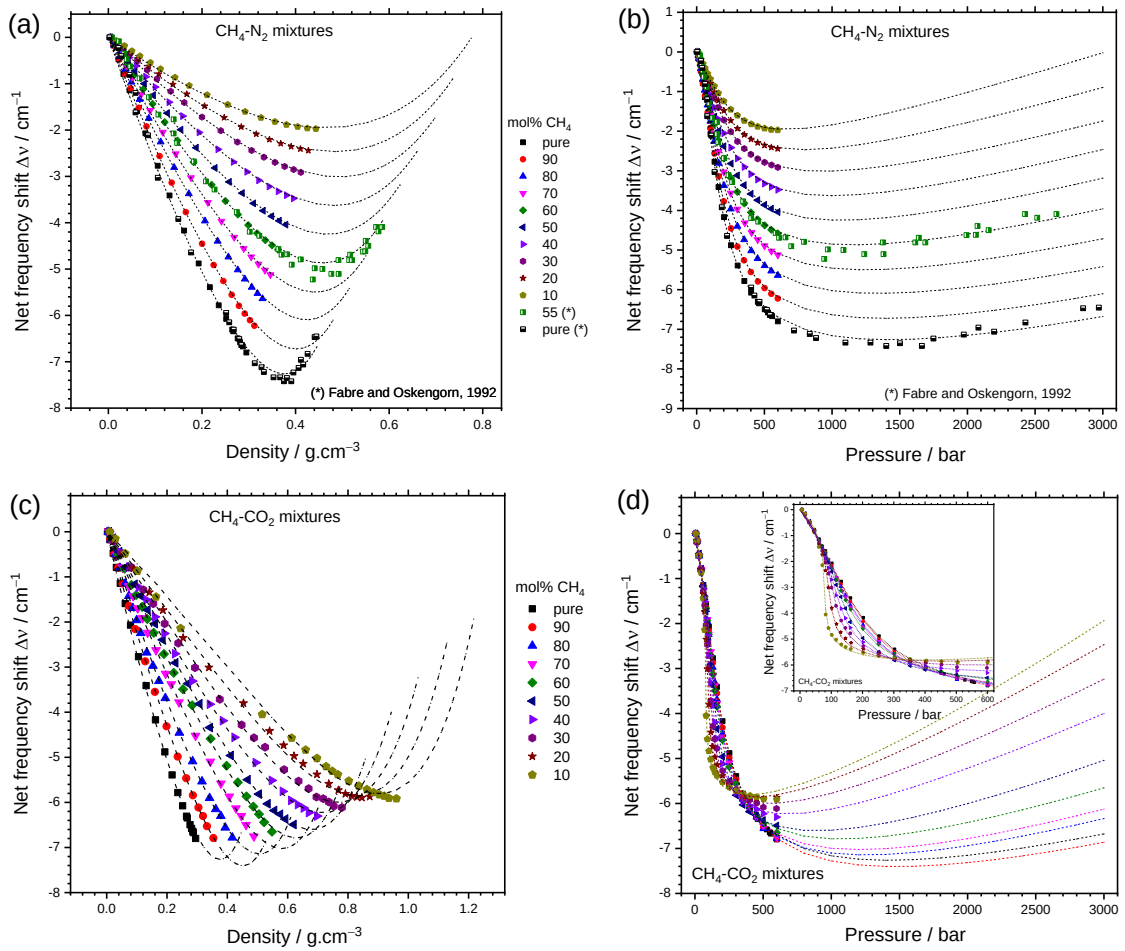


Figure 7: Variation of the net predicted frequency shift ($\Delta\nu$) of the $CH_4$ $\nu_1$ band (at 22 °C) as a function of composition and density (a, c) or pressure (b, d) within $CH_4$-$N_2$ and $CH_4$-$CO_2$ mixtures. The predicted frequency shift is represented by dashed lines. The experimental data from Le et al. [17] and Fabre and Oksengorn [11] are represented by symbols.

Talking about the uncertainty of the predictive model, the hard-sphere diameters of solvent ($\sigma_s$) are the most sensitive parameter in the PHF model which are calculated with an uncertainty of about ± 2%.[34] This corresponds to a fluctuation of about 0.1 $cm^{-1}$ on the predicted frequency shift value. There are also other possible sources of inaccuracy not quantified yet such as the uncertainty of the attractive parameters and the error due to extrapolation to a wider pressure-range where no experimental data exist. Indeed, $\Delta\nu_A$ were fitted from experimental data by a quadratic density-dependence, but not a linear one. Most of the experimental data used herein were obtained at ≤ 600 bars. Thus, extrapolation to 3000 bars from the best-fitted quadratic function could obviously cause more or less deviation in the predicted curves, depending on its curvature. Thereby, the predictive model of $CH_4$-$CO_2$ mixtures is expected to have a larger error than that of $CH_4$-$N_2$ mixtures because the non-linearity of the $\Delta\nu_A$ density-dependence within $CH_4$-$CO_2$ mixtures is more important than within $CH_4$-$N_2$ mixtures (see text above and Figure 6a and b). Also, an irregular distance between the fitted curves (cf. Figure 6d) and an inversion of the order of the predicted curves with composition of 100% and 90% $CH_4$ (cf. Figure 7d) indicate that the predictive model of $CH_4$-$CO_2$ mixtures still contains an appreciable error at high pressure, which should not be negligible upon quantitative measurements requiring high precision. Thus, further experimental data at elevated pressure range are still needed to refine and obtain higher accurate predictive models, especially for the $CH_4$-$CO_2$ mixtures dominated by $CO_2$. Overall, the predictive model of the frequency shift presented in this study can still hold and could be used to reasonably predict the variation trend of the $CH_4$ $\nu_1$ band within binary mixtures.

## Conclusions

The variation of the peak position of the $\nu_1$ stretching band of $CH_4$ and $N_2$ within different non-polar solutions (i.e., pure $CH_4$, pure $N_2$, and binary mixtures of $CH_4$ with $CO_2$ or $N_2$), where attraction and repulsion are the major intermolecular interaction forces, was intuitively interpreted based on the basic of the Lennard-Jones 6-12 potential approximation,

without any complex *ab-initio* calculations or molecular dynamics simulations. Thereby, the redshift and blueshift of the $CH_4$ and $N_2$ $\nu_1$ band as varying pressure (density) were reasonably attributed to the contribution of the variation of attractive and repulsive forces, simply as a function of intermolecular distance *r*. The experimental results reported in this study surprisingly showed a very close affinity between the variation trend of the Raman peak position and the variation of the net LJ potential, especially the superposition of inflection points A and B observed on LJ potential curves and Raman frequency shifts curves upon an isotherm increase of pressure or density. This is the evidence of the intrinsic correlation of the Raman peak position variation and the intermolecular interaction change. The LJ potential approximation could also practically point out the difference in the length scale of the intermolecular interaction forces exercising within $CH_4$-$N_2$ and $CH_4$-$CO_2$ gas mixtures, i.e., the molecules within $CH_4$-$N_2$ mixtures experience longer distance-range forces than that within $CH_4$-$CO_2$ mixtures at a given pressure at 22 °C, even though in both cases the attractive forces always dominate the net intermolecular forces, resulting in a redshift over the studied pressure range.

The shortcoming of the LJ 6-12 potential approximation in the interpretation of Raman frequency shift of the $CH_4$ $\nu_1$ band as a function of composition (i.e., the molar proportion of solute and solvent) is completed by using the generalized PHF model. It was successfully applied to $CH_4$-$N_2$ and $CH_4$-$CO_2$ binary mixtures of any molar fraction to quantitatively investigate the solute-solvent interactions. The observed frequency shift of the $CH_4$ $\nu_1$ band could therefore be decomposed into attractive and repulsive components, which are induced by the attractive and repulsive solvation mean-forces, respectively. The predicted model of the variation trend of the $CH_4$ $\nu_1$ band position within $CH_4$-$N_2$ and $CH_4$-$CO_2$ mixtures could also be provided over 5 - 3000 bars. Moreover, the experimental and predicted data over a wide composition-range revealed some interesting information. The change in the solvation-induced attractive component is responsible for the change of frequency shift of the $CH_4$ $\nu_1$ band in $CH_4$-$N_2$ mixtures (Figure 6c), whereas that in $CH_4$-$CO_2$ mixtures is governed by the change of the solvation-induced repulsive component (Figure 6d). Also, the slight non-linear density dependence of the frequency shift of the C-H bond of $CH_4$ was evaluated and confirmed. It was clearly shown that the frequency shift of the same type of bond (herein C−H in $CH_4$ molecules) strongly depends on solvent parameters as well as the composition of the solution. Overall, the study conducted herein illustrates the practicality and reliability of Raman spectroscopy for investigating thermodynamic and intermolecular behavior of gaseous molecule systems at the molecular scale, which could be an alternative way to directly and quickly determine or estimate intermolecular forces, relative bond length changes,[39] and other quantitative measurements as shown in previous works such as physical properties of gas mixtures with a good accuracy (after a specific calibration of the Raman signal) , e.g., *PVTX* properties [16–18,45], fugacity and fugacity coefficients [18,46].

## Conflicts of interest

There are no conflicts to declare

## Acknowledgements

The authors acknowledge the French Ministry of Education and Research and the ICEEL Institut Carnot. The work benefited of financial support from CNRS-INSU CESSUR program. Two anonymous reviewers are thanked for their thorough and constructive reviews.

## Notes and references

1 D. A. Long, *The Raman Effect : A Unified Treatment of the Theory of Raman Scattering by Molecules*, 2002.

2 P. Rostron and D. Gerber, Raman Spectroscopy, a review, *International Journal of Engineering and Technical Research*, 2016, **6**, 50–64.

3 G. Placzek, *Rayleigh-Streuung und Raman-Effekt*, Akad. Verlag-Ges., 1934, vol. 2.

4 A. D. Buckingham, A theory of frequency, intensity and band-width changes due to solvents in infra-red spectroscopy, *Proc. R. Soc. Lond. A*, 1960, **255**, 32–39.

5 K. S. Schweizer and D. Chandler, Vibrational dephasing and frequency shifts of polyatomic molecules in solution, *The Journal of chemical physics*, 1982, **76**, 2296–2314.

6 J. Mullis, The system methane-water as a geological thermometer and barometer from the external part of the Central Alps, *Bull Minéral*, 1979, **102**, 526–536.

7 E. Roedder, Fluid Inclusions. Reviews in Mineralogy, *Mineral. Soc. Am.*, 1984, **12**, 644.

8 J. Mullis, J. Dubessy, B. Poty and J. O'Neil, Fluid regimes during late stages of a continental collision: Physical, chemical, and stable isotope measurements of fluid inclusions in fissure quartz from a geotraverse through the Central Alps, Switzerland, *Geochim Cosmochim Acta.*, 1994, **58**, 2239–2267.

9 A. Tarantola, J. Mullis, T. Vennemann, J. Dubessy and C. de Capitani, Oxidation of methane at the CH4/H2O–(CO2) transition zone in the external part of the Central Alps, Switzerland: Evidence from stable isotope investigations, *Chem. Geol.*, 2007, **237**, 329–357.

10 C. H. Wang and R. B. Wright, Effect of density on the Raman scattering of molecular fluids. I. A detailed study of the scattering polarization, intensity, frequency shift, and spectral shape in gaseous $N_2$, *J. Chem. Phys.*, 1973, **59**, 1706–1712.

11 D. Fabre and B. Oksengorn, Pressure and Density Dependence of the CH4 and N2 Raman Lines in an Equimolar CH4/N2 Gas Mixture, *Appl. Spectrosc., AS*, 1992, **46**, 468–471.

12 V. Thieu, S. Subramanian, S. O. Colgate and E. D. Sloan, High-Pressure Optical Cell for Hydrate Measurements Using Raman Spectroscopy, *Annals of the New York Academy of Sciences*, 2000, **912**, 983–992.

13 Lin, R. J. Bodnar and S. P. Becker, Experimental determination of the Raman CH4 symmetric stretching (v1) band position from 1–650bar and 0.3–22°C: Application to fluid inclusion studies, *Geochim Cosmochim Acta.*, 2007, **71**, 3746–3756.

14 J. C. Seitz, J. D. Pasteris and I.-M. Chou, Raman spectroscopic characterization of gas mixtures; I, Quantitative composition and pressure determination of CH 4, N 2 and their mixtures, *Am. J. Sci.*, 1993, **293**, 297–321.

15 J. C. Seitz, J. D. Pasteris and I.-M. Chou, Raman spectroscopic characterization of gas mixtures. II. Quantitative composition and pressure determination of the CO2-CH4 system, *Am. J. Sci.*, 1996, **296**, 577–600.

16 V.-H. Le, M.-C. Caumon, A. Tarantola, A. Randi, P. Robert and J. Mullis, Quantitative Measurements of Composition, Pressure, and Density of Microvolumes of CO2–N2 Gas Mixtures by Raman Spectroscopy, *Anal. Chem.*, 2019, **91**, 14359–14367.

17 V.-H. Le, M.-C. Caumon, A. Tarantola, A. Randi, P. Robert and J. Mullis, Calibration data for simultaneous determination of P-V-X properties of binary and ternary CO2 - CH4 - N2 gas mixtures by Raman spectroscopy over 5–600 bar: Application to natural fluid inclusions, *Chemical Geology*, 2020, **552**, 119783.

18 D. M. Sublett, E. Sendula, H. M. Lamadrid, M. Steele-MacInnis, G. Spiekermann and R. J. Bodnar, Raman spectral behavior of N2, CO2, and CH4 in N2–CO2–CH4 gas mixtures from 22°C to 200°C and 10 to 500 bars, with application to other gas mixtures, *Journal of Raman Spectroscopy*, , DOI:https://doi.org/10.1002/jrs.6033.

19 J. E. Jones and S. Chapman, On the determination of molecular fields. —II. From the equation of state of a gas, *Proceedings of the Royal Society of London. Series A, Containing Papers of a Mathematical and Physical Character*, 1924, **106**, 463–477.

20 D. Ben-Amotz and D. R. Herschbach, Hard fluid model for solvent-induced shifts in molecular vibrational frequencies, *J. phys. chem. (1952)*, 1993, **97**, 2295–2306.

21 D. Ben-Amotz, F. LaPlant, D. Shea, J. Gardecki and D. List, in *Supercritical Fluid Technology*, American Chemical Society, 1992, vol. 488, pp. 18–30.

22 E. J. Hutchinson and D. Ben-Amotz, Molecular Force Measurement in Liquids and Solids Using Vibrational Spectroscopy, *J. Phys. Chem. B*, 1998, **102**, 3354–3362.

23 I.-M. Chou, R. C. Burruss and W. Lu, in *Advances in High-Pressure Technology for Geophysical Applications*, eds. J. Chen, Y. Wang, T. S. Duffy, G. Shen and L. F. Dobrzhinetskaya, Elsevier, Amsterdam, 2005, pp. 475–485.

24 M.-C. Caumon, P. Robert, E. Laverret, A. Tarantola, A. Randi, J. Pironon, J. Dubessy and J.-P. Girard, Determination of methane content in NaCl–H2O fluid inclusions by Raman spectroscopy. Calibration and application to the external part of the Central Alps (Switzerland), *Chem. Geol.*, 2014, **378**, 52–61.

25 E. W. Lemmon, M. L. Huber and M. O. McLinden, NIST Standard Reference Database 23: Reference Fluid Thermodynamic and Transport Properties-REFPROP, Version 9.1, National Institute of Standards and Technology, *Standard Reference Data Program, Gaithersburg*.

26 U. Setzmann and W. Wagner, A New Equation of State and Tables of Thermodynamic Properties for Methane Covering the Range from the Melting Line to 625 K at Pressures up to 100 MPa, *Journal of Physical and Chemical Reference Data*, 1991, **20**, 1061–1155.

27 R. Span, E. W. Lemmon, R. T. Jacobsen, W. Wagner and A. Yokozeki, A Reference Equation of State for the Thermodynamic Properties of Nitrogen for Temperatures from 63.151 to 1000 K and Pressures to 2200 MPa, *Journal of Physical and Chemical Reference Data*, 2000, **29**, 1361–1433.

28 O. Kunz and W. Wagner, The GERG-2008 Wide-Range Equation of State for Natural Gases and Other Mixtures: An Expansion of GERG-2004, *J. Chem. Eng. Data*, 2012, **57**, 3032–3091.

29 H. M. Lamadrid, L. R. Moore, D. Moncada, J. D. Rimstidt, R. C. Burruss and R. J. Bodnar, Reassessment of the Raman CO2 densimeter, *Chem. Geol.*, 2017, **450**, 210–222.

30 D. Möller, J. Óprzynski, A. Müller and J. Fischer, Prediction of thermodynamic properties of fluid mixtures by molecular dynamics simulations: methane-ethane, *Molecular Physics*, 1992, **75**, 363–378.

31 J. O. Hirschfelder, C. F. Curtiss and R. B. Bird, *Molecular theory of gases and liquids*, 1964, vol. 165.

32 M. R. Zakin and D. R. Herschbach, Vibrational frequency shifts induced by molecular compression of pyridine in solution, *J. Chem. Phys.*, 1986, **85**, 2376–2383.

33 Lin, A. K. Sum and R. J. Bodnar, Correlation of methane Raman v1 band position with fluid density and interactions at the molecular level, *Journal of Raman Spectroscopy*, 2007, **38**, 1510–1515.

34 D. Ben-Amotz, M. Lee, S. Y. Cho and D. J. List, Solvent and pressure-induced perturbations of the vibrational potential surface of acetonitrile, *J. Chem. Phys.*, 1992, **96**, 8781–8792.

35 F. G. Dijkman and J. H. van der Maas, Inhomogeneous broadening of Morse oscillators in liquids, *J. Chem. Phys.*, 1977, **66**, 3871–3878.

36 M. R. Zakin and D. R. Herschbach, Density dependence of attractive forces for hydrogen stretching vibrations of molecules in compressed liquids, *The Journal of Chemical Physics*, 1988, **89**, 2380–2387.

37 G. S. Devendorf and D. Ben-Amotz, Vibrational frequency shifts of fluid nitrogen up to ultrahigh temperatures and pressures, *The Journal of Physical Chemistry*, 1993, **97**, 2307–2313.

38 M. Lee and D. Ben-Amotz, Pressure induced vibrational frequency shifts of ethane and methyliodide. Evidence for the formation of C–H hydrogen bonds in high density fluids, *J. Chem. Phys.*, 1993, **99**, 10074–10077.

39 Y. Meléndez-Pagán and D. Ben-Amotz, Intermolecular Forces and Bond Length Changes in High-Pressure Fluids. Vibrational Spectroscopic Measurement and Generalized Perturbed Hard Fluid Analysis, *J. Phys. Chem. B*, 2000, **104**, 7858–7866.

40 K. Saitow, H. Nakayama, K. Ishii and K. Nishikawa, Attractive and Repulsive Intermolecular Interactions of a Polar Molecule: Short-Range Structure of Neat Supercritical CHF3 Investigated by Raman Spectroscopy, *J. Phys. Chem. A*, 2004, **108**, 5770–5784.

41 D. Kajiya and K. Saitow, Investigation of attractive and repulsive interactions associated with ketones in supercritical CO2, based on Raman spectroscopy and theoretical calculations, *J. Chem. Phys.*, 2013, **139**, 054509.

42 W. F. Murphy, W. Holzer and H. J. Bernstein, OSA | Gas Phase Raman Intensities: A Review of "Pre-Laser" Data, https://www.osapublishing.org/as/abstract.cfm?uri=as-23-3-211, (accessed June 25, 2018).

43 R. Hellmann, E. Bich, E. Vogel and V. Vesovic, Intermolecular potential energy surface and thermophysical properties of the CH4–N2 system, *J. Chem. Phys.*, 2014, **141**, 224301.

44 A. Kramida, Y. Ralchenko, J. Reader and NIST ASD Team, *NIST Atomic Spectra Database (version 5.6.1)*, 2018.

45 D. M. Sublett, E. Sendula, H. Lamadrid, M. Steele-MacInnis, G. Spiekermann, R. C. Burruss and R. J. Bodnar, Shift in the Raman symmetric stretching band of N2, CO2, and CH4 as a function of temperature, pressure, and density, *Journal of Raman Spectroscopy*, 2020, **51**, 555–568.

46 H. M. Lamadrid, M. Steele-Macinnis and R. Bodnar, Relationship between Raman spectral features and fugacity in mixtures of gases, *J. Raman Spectrosc.*, , DOI:10.1002/jrs.5304.